International Journal of Thermophysics, Vol. 11, No. 4, 1990

Extension of Thermophysical and Thermodynamic Property Measurements by Laser Pulse Heating up to 10,000 K. I. Under Pressure[1]

R. W. Ohse[2,3]

The necessity for increased high-temperature data reliability and extension of thermophysical property measurements up to 5000 K and above are discussed. A new transient-type laser-autoclave technique (LAT) has been developed to extend density and heat capacity measurements of high-temperature multicomponent systems far beyond their melting and boiling points. Pulsed multibeam laser heating is performed in an autoclave under high inert gas pressure to eliminate evaporation. The spherical samples are positioned by containment-free acoustic levitation regardless of their conductive or magnetic properties. Temperature, spectral and total emittances are determined by a new microsecond six-wavelength pyrometer coupled to a fast digital data acquisition system. The density is determined by high resolution microfocus X-ray shadow technique. The heat capacity is obtained from the cooling rate. Further applications are a combination of the laser-autoclave with splat cooling techniques for metastable structure synthesis and amorphous metals research and an extension of the LAT for the study of critical phenomena and the measurement of critical-point temperatures.

KEY WORDS: acoustic levitation; autoclave technique; density; emissivity; heat capacity; high temperatures; laser pulse heating; pyrometry; thermal expansion; transient pulse heating; X-ray shadow technique.

[1] Paper presented at the First Workshop on Subsecond Thermophysics, June 20–21, 1988, Gaithersburg, Maryland, U.S.A.

[2] Commission of the European Communities, Joint Research Center, Karlsruhe Establishment, European Institute for Transuranium Elements, Postfach 2340, D-7500 Karlsruhe, Federal Republic of Germany.

[3] Present address: Weinbergstrasse 4, D-7770 Überlingen/Bodensee, Federal Republic of Germany.

0195-928X/90/0700-0753$06.00/0

1. INTRODUCTION

Future progress in high-temperature technologies depends largely on the materials' performance and on the availability of reliable thermophysical, thermochemical, and thermodynamic high-temperature data [1]. This is of extreme importance at very high temperatures, where data can differ dramatically from predictions based on the extrapolation of low-temperature data [2–7].

High-temperature materials research has been concentrated on the development of materials able to withstand the environments and stresses imposed by modern technologies on improving mechanical properties under large temperature gradients such as thermal shock resistance and tensile strength at adequate chemical stability. The rapidly increasing fuel costs and need for improved thermal efficiency of engines and power plants and the growing demand for limiting air pollution led to large-scale conversion of energy resources (fission and fusion reactors [8–10], solar power plants [11], electrochemical energy storage [12], coal conversion and MHD power generation [13], etc.) and increase in the operating and peak temperature of the cycles [14] and consequently to the necessity of extending our knowledge on materials' properties to higher temperatures. Every aspect of energy production, its extraction, processing, refining, and conversion, depends on materials' performance matched to the needs of the process. This can be achieved only by improved designs and better materials, i.e., progress and innovations in materials science [1].

The necessity for increased high-temperature data reliability has led to an extension and refinement of theoretical models [4, 5, 7, 15–17]. Large computational facilities [18, 19] are needed to simulate and investigate the structure of liquids and ionic and molecular or intermolecular models, thus allowing a closer reproduction of thermophysical properties and better accuracy of the predicted data. Although the reliability of fundamental approaches based on computer simulations, such as the Monte Carlo technique [20] or the method of molecular dynamics [21], is limited only by the applicability of the chosen model potential for a given substance, the selection of a realistic potential may present a problem.

The extension of property measurements to very high temperatures [1, 4, 5, 10, 22] leads to severe problems such as rapid increase in heat transfer, chemical reactivity, high rates of evaporation, and loss of materials strength imposing short heating times by transient dynamic pulse-heating techniques [4, 5, 10, 22] and fast digital data acquisition systems. The problems and requirements of high-temperature property measurements are discussed in Section 2. The laser-autoclave technique (LAT) as a new approach of transient-type laser pulse heating under

pressure (LHP) is demonstrated in Sections 3 to 6 on the extension of density and heat capacity measurements of multicomponent systems up to 5000 K and above.

2. PROBLEMS AND REQUIREMENTS AT VERY HIGH TEMPERATURES

The problems faced at very high temperatures are due largely to the complex materials' behavior at these temperatures and its consequences on measurement.

2.1. Materials Behavior at Very High Temperatures

The extension of thermophysical and thermodynamic property measurements to very high temperatures leads to a number of severe materials' phenomena ranging from compositional changes and extreme rates of evaporation to charged particle emission and thermal ionisation [4, 22, 25].

For temperatures up to 2500 K chemical reactivity, rate of evaporation, compositional changes, increase in heat transfer, temperature uniformity, and loss of material strength are of primary importance. The increase in chemical reactivity needs careful control of the compatibility of sample and container materials, the solid–liquid and liquid–gas reactions, and the kinetics of such high-temperature processes. Impurities, porosity, grain size and segregation effects, nucleation, and growth may, in addition, have a profound effect on the property and its measurement. High rates of evaporation of multicomponent systems lead to surface depletion of the more volatile component and eventually to changes in the bulk composition. Compositional changes and phase transformations must thus be checked by chemical and structural analysis. The range of crucible materials is limited to refractory metals and ceramics such as tungsten, tantalum, molybdenum and borides, carbides, nitrides, oxides, and silicides or to graphite. Most property measurements can, however, still be performed under stationary, steady-state, or quasi-steady-state conditions in or close to thermodynamic equilibrium.

A further increase in temperature to 5000 and 10,000 K leads to extreme rates of evaporation, charged particle emission, and a drastic increase in chemical reactivity, imposing short heating times by dynamic pulse-heating techniques and self-contained or containment-free sample heating by levitation techniques. Additional constraints are due to non-uniformity in heating or energy absorption leading to large radial and axial temperature gradients and expansion forces in the condensate [10]. The

various problems have to be eliminated or their effects accurately enough accounted for by introducing sufficiently high spatial and temporal resolution into the experimental high-speed diagnostics.

2.2. Temperature and Emissivity Measurements by Microsecond Six-Wavelength Pyrometry

Multi-wavelength pyrometer are used to overcome the problem of unknown emissivity and transmissivity. In single-color pyrometry the spectral emittance (depending on the state of the actual surface and the material constant, the emissivity) at the wavelength of measurement has to be known. In two-color pyrometry the ratio of the emittances at the two wavelengths must be constant. In three-color pyrometry the variation of the spectral emittance with wavelength can be linear. The requirements of transient pulse-heating techniques and rapid advances in fast digital data acquisition and fiber optics have led to the construction of a new generation of ultrafast six-wavelength pyrometer capable of measuring the quantity of light emitted by a surface of unknown emittance at different wavelengths with high spatial and temporal resolution [26–28]. Measurements at six wavelengths are necessary to determine reliably the emittance dependence on wavelength at constant temperature necessary to calculate the required total emittance [1, 23, 29] in Section 6. For transient dynamic pulse-heating experiments a simultaneous measurement at all six wavelengths was found necessary because of the fast temperature changes and the nonreproducibility in temperature at subsequent shots, due to slight variations in the sample surface and pulse energy.

2.2.1. Theoretical Background

Temperature and emissivity measurements above the gold point are based on the Wien equation,

$$J_B(\lambda, T) = C_1 \lambda^{-5} \exp(-C_2/\lambda T) \tag{1}$$

where $J_B(\lambda, T)$, C_1, and C_2 are the light flux of a blackbody and the radiation constants. The light flux of a real body J_R depends on the emissivity $\varepsilon(\lambda, T)$ according to

$$J_R(\lambda, T) = \varepsilon(\lambda, T)\, J_B(\lambda, T) = J_B(\lambda, T_R) \tag{2}$$

where T_R and T are the spectral radiance temperature and the true temperature. Equations (1) and (2) lead to the basic working equation of optical pyrometry

$$\lambda \ln \varepsilon(\lambda, T)/C_2 = 1/T - 1/T_R \tag{3}$$

which relates the emissivity, the spectral radiance temperature, and the true temperature. In practice the detector sensitivity, geometry, absorption through windows, and first radiation constant C_1 are taken into account in the calibration factor A_λ, which depends on wavelength but not on temperature. The relation between the output signal $V(\lambda, T)$ of the detector and the light flux $J_R(\lambda, T)$ of a real body is given by

$$V(\lambda, T) = A_\lambda J_R(\lambda, T) \tag{4}$$

The variation of the spectral emissivity with wavelength over a small enough range can be expressed as

$$\ln \varepsilon(\lambda, T) = a + b\lambda \tag{5}$$

where a and b are functions of temperature. Combining Eqs. (4), (5), and (2) leads to

$$V(\lambda, T) = A_\lambda \exp(a + b\lambda)\, \lambda^{-5} \exp(-C_2/\lambda T) \tag{6}$$

Taking the logarithm and rearranging gives

$$\ln[V(\lambda, T)]\lambda^5/A_\lambda) = -C_2/\lambda T + a + b\lambda \tag{7}$$

Applying Eq. (7) at two wavelengths λ_1 and λ_2 and subtracting leads to

$$\frac{1}{\lambda_1 - \lambda_2}\left\{\ln\left[\frac{V(\lambda_1, T)\,\lambda_1^5}{A_{\lambda_1}}\right] - \ln\left[\frac{V(\lambda_2, T)\,\lambda_2^5}{A_{\lambda_2}}\right]\right\} = (C_2/T)(1/\lambda_1\lambda_2) + b \tag{8}$$

A plot of the left part of Eq. (8) against $1/\lambda_1\lambda_2$ gives a straight line. With six wavelengths, the pairwise combination leads to 15 equations of type (8), from which T can be determined by a least-squares analysis. Rearranging Eq. (6) and taking the logarithm gives

$$\ln \varepsilon(\lambda, T) = \ln[V(\lambda, T)\lambda^5/A_\lambda] - C_2/\lambda T \tag{9}$$

The six values of $\varepsilon(\lambda, T)$ at six wavelengths give the coefficients a and b in Eq. (5). With T and $\varepsilon(\lambda, T)$ known as a function of λ the total emissivity ε_t can be calculated from

$$\varepsilon_t(T) = \int_0^\infty \varepsilon(\lambda, T)\, \lambda^{-5} \exp(-C_2/\lambda T)\, d\lambda \Big/ \int_0^\infty \lambda^{-5} \exp(-C_2/\lambda T)\, d\lambda \tag{10}$$

The integration can be done within a finite wavelength range where the limits λ_1 and λ_2 should be selected such that the main flux emitted by a blackbody at temperature T is included.

2.2.2. *Pyrometer Requirements*

The main requirements of optical pyrometry for thermophysical property measurements by transient pulse heating techniques are

high-temperature resolution of better than 1% at 5000 K,
microsecond time resolution,
high spatial resolution to keep within 1% of temperature variation over the measured area, and
simultaneous measurement at different wavelengths to determine the variation of spectral emissivity with wavelength and temperature and to permit the calculation of the total emissivity.

The conditions for the applicability of the calculation procedure for the six-wavelength pyrometer are that

the stability and linearity of the detector response must be better than 1% and
the straight line obtained from the 15 equations of type (8) must have a confidence limit of at least 0.999.

2.2.3. *Optical Concept*

The optical concept is given in Fig. 1. An image of the heated surface is given on the microaperture (first field stop) of the pyrometer. The

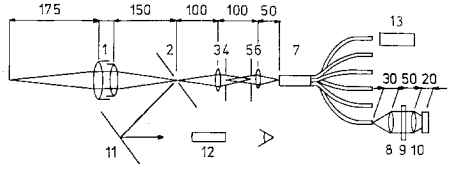

Fig. 1. Optical display of microsecond six-wavelength pyrometer. (1) Entrance objective ($f = 90$–120 mm). (2) First field stop (diameter, 1.5 mm). (3) Intermediate lens ($f = 80$ mm). (4) Effective aperture stop. (5) Main field stop (diameter, 1.0 mm). (6) Field lens producing image of effective aperture stop on fiber-glass bundle. (7) Fiber-glass bundle for light splitting. (8) Lenses for focusing light on detector and producing parallel light beams through interference filters ($f = 30$ mm). (9) Interference filters (six). (10) Detector (six EG & G Si photo diodes HUV-4000 B). (11, 12) Mirrors and telescope for image observation on microaperture 2 and entrance of glass-fiber bundle. (13) HeNe laser for optical alignment.

microaperture diameter of the first field stop and the magnification of the imaging system determine the spatial resolution of the pyrometer. The image of the effective aperture stop is produced by a field lens, placed behind the main field stop, at the entrance of the fiber-glass bundle. The light is then split and conducted through the fiber-glass system and six interference filters onto six silicon photodiodes (EG & G, Type HUV 4000 B) with a spectral response range from 450 to 1100 nm. A HeNe laser is used for optical alignment.

2.3. Transient Dynamic Pulse-Heating Technique

The main techniques developed for the extension of property measurements up to 5000 and 10,000 K can be subdivided into chemical flames, exploding wire, shockwave, imaging and solar heating, electrical discharge, fission/fusion, and high-energy electron and laser heating. An adaptation of classical heating techniques such as resistance, induction, and electron bombardment heating to very high temperatures is rather limited. The four main approaches suited for ultrashort pulse heating, isobaric resistive heating (exploding wire technique), and electron, neutron, and laser pulse heating have been summarized before [4, 5, 10]. For the extension of property measurements to very high pressures, using techniques such as laser-driven shock-wave loading (adiabatic compression), reference is given to the excellent reviews by Gather [30] and Ross [31].

Each of these transient pulse heating techniques was found to introduce its own experimental and interpretational problems [4, 5, 10], giving rise to specific requirements in order to guarantee adequate reliability and accuracy in property measurements. The appropriate technique is selected on behalf of the property to be determined. The investigation of the vaporization behaviour of multicomponent systems as described in the following paper [32], i.e., the mass spectrometric determination of the gaseous species and their partial pressures, requires evaporation into vacuum. Here heating can be restricted to the surface region, which, at extreme temperatures is even advisable to avoid entering into a "burst mode" regime [5]. The same applies to all surface properties such as spectral and total emittances, surface tension, etc. Measurements of volume properties such as density, thermal expansion, enthalpy, and heat capacity rely on the achievement of temperature uniformity or the accurate knowledge of the temperature profile throughout the sample. In order to eliminate vaporization laser pulse heating is performed in an autoclave (Fig. 2) under high inert gas pressure as described in Sections 3 to 6.

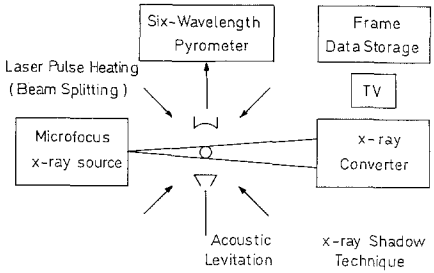

Fig. 2. Laser-autoclave technique (LAT) as a combination of pulsed multibeam laser heating under pressurized inert gas atmosphere, six-wavelength pyrometry, X-ray shadow technique, and containment-free acoustic levitation.

3. LASER-AUTOCLAVE TECHNIQUE (LAT): EXPERIMENTAL APPROACH

The new laser-autoclave technique (Fig. 2) [1, 10, 23, 24], as a combination of pulsed multibeam laser heating under pressurized inert gas atmosphere, six-wavelength pyrometry, high-resolution microfocus X-ray shadow technique, and containment-free acoustic levitation, has first been developed to extend thermophysical property measurements (heat capacity, density, thermal expansion, spectral and total emissivity, etc.) far beyond the melting and boiling point of ceramic fuel materials regardless of their conductive or magnetic properties [1, 10, 23, 24].

The heat capacity is obtained from the cooling rate. A spherical sample (e.g., UO_2) is heated by four 100-ms laser beams of two Nd doped solid-state YAG lasers up to temperatures of the order of 5000 K applying beam splitting in a tetrahedral configuration as shown in Fig. 3. After switching off the laser pulse heating the temperature is measured as a function of time. In principle the heat loss during cooling is given by the loss through vaporization, radiation, and convection. In order to eliminate heat losses by vaporization, i.e., restrict to radiation and convection as the only heat loss mechanisms, laser pulse heating is performed in an autoclave (Fig. 4) with sapphire windows under an adequate high inert gas pressure. The spatial focal laser power profile is measured by profile detectors consisting of a TV camera, frame storage, and single line display on a storage oscilloscope. The laser beam adjustment is controlled by an infrared sensitive TV camera applying the same frame storage device as used for profile detection (Fig. 3). The cooling rate and spectral and total emittances are measured by a submillisecond six-wavelength pyrometer described in

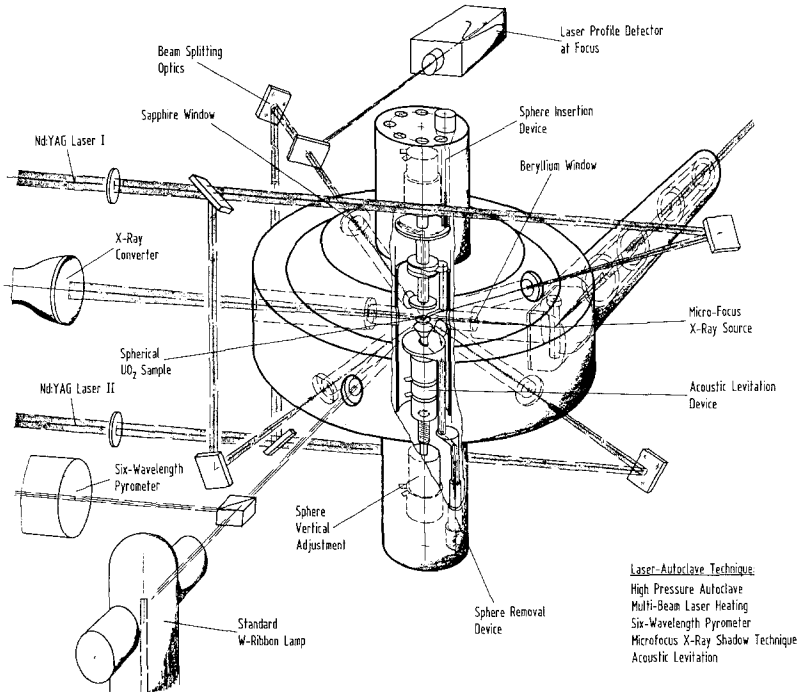

Fig. 3. Perspective drawing of tetrahedral laser pulse heating of spherical samples within a high-pressure autoclave, showing acoustic levitation, pyrometry, and X-ray shadow technique.

Section 2.2. The diameter, thermal expansion, and density display of the liquid sphere during the heating and cooling cycles are measured by a high-resolution microfocus X-ray shadow technique. It consists of a microfocus X-ray converter with image intensifier, TV camera, monitor display, and frame data storage. The spherical liquid metallic or ceramic samples are suspended by acoustic levitation [1, 23, 24]. A flat levitator (vibrator) and curved reflector, adjusted within the vertical central channel of the autoclave (Fig. 4), are piezoelectrically driven by an ultrasonic piston transducer operating at a resonance frequency between 50 and 80 kHz with a 12-mm-diameter radiating front face. The sphere is levitated by the axial and stabilized by the radial gradients of sound pressure within the tuned standing resonance wave pattern. Density changes of the inert gas around the levitated sphere during the transient laser pulse heating may effect the stability of this standing resonance wave pattern. An adequate radial stability by increased radial retaining forces is necessary to compensate these instabilities.

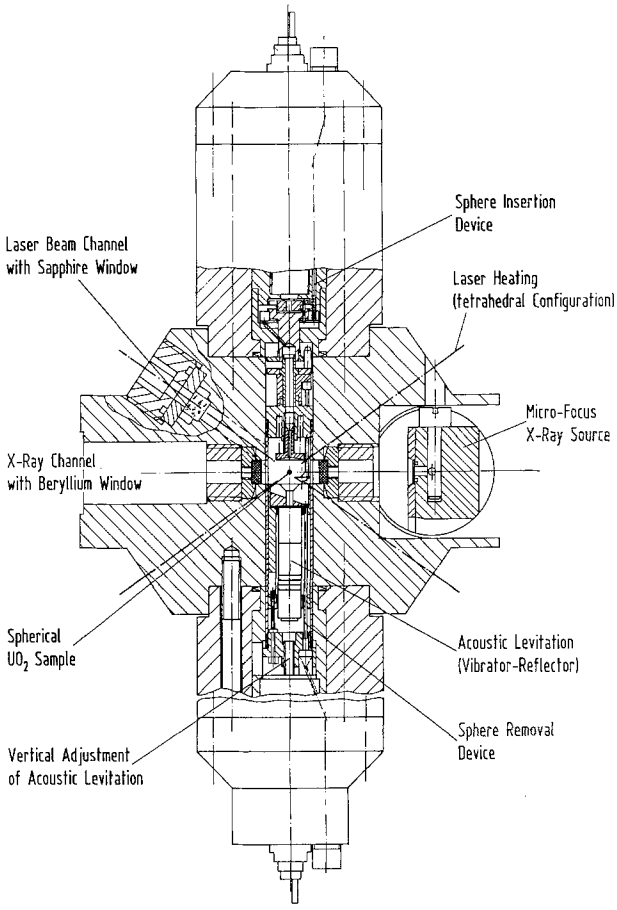

Fig. 4. Cross section of high pressure laser-autoclave.

4. ACCURACY REQUIREMENTS

Heat capacity and density data of the liquid nuclear fast-breeder oxide fuels are required for safety risk assessment up to at least 5000 K. The heat capacity of the fuel affects both the Doppler and the disassembly feedbacks. It relates the energy to the temperature attained during an excursion and permits the calculation of the amount of energy required before melting occurs. According to numerous sensitivity studies of excursion yields [4, 5, 10, 33–40] the heat capacity of the fuel material [41, 42] should be known within $\pm 10\%$. The density is required to calculate the negative reactivity feedback as the volume increases with temperature, in particular

upon melting and beyond. Because of the high sensitivity of the heat capacity on volume, liquid density data in this special application are required within $\pm 2\%$ ($\Delta\rho/\rho = \pm 0.02$), implying an allowable error of 0.67% in the determination of the diameter of the sphere (23). Hence the maximum allowable uncertainties in diameter for spheres 500 to 1000 μm in diameter are 3.4 to 6.7 μm.

5. DENSITY MEASUREMENT

A high resolution X-ray shadow technique has been chosen as the best available diagnostic technique for the determination of the time-resolved expansion of the microspheres [1, 23]. The X-ray shadow technique consists of a microfocus X-ray source, X-ray converter with image intensifier, TV camera, monitor display, and frame data storage. The resolution depends mainly on the spot diameter of the X-ray source, magnification factor, and resolution of the converter foil. The overall magnification is given by the ratio of the focal distances of the image plane to that of the object plane. The focal distance of the image plane is limited by the available X-ray intensity. The X-ray tube head of the X-ray unit has therefore been placed as close as possible to the sphere (Fig. 4; approx 60 mm). The required resolution of the order of 1–5 μm is obtained by an X-ray microfocus 1–5 μm in diameter and a magnification up to 40 times the

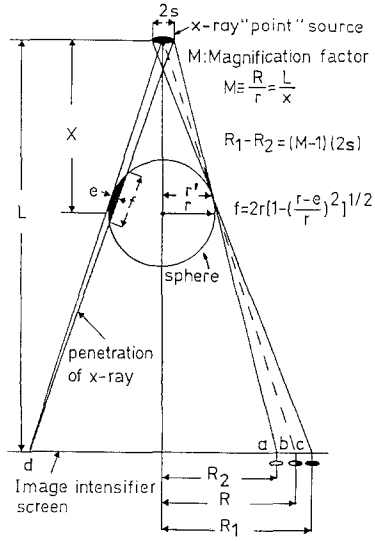

Fig. 5. Schematic diagram of the X-ray shadow technique.

sphere diameter on the X-ray converter. A reduction of the focal distance of the image plane can be achieved by an improvement of the resolution of the converter foil.

The three main problems are the finite size of the "point" X-ray source, the absorption of X-rays in the high-pressure inert gas (Ar), and the diffuse image of the sphere caused by the penetration of high-energy X-rays through the sphere periphery. The finite size of the X-ray source produces a "half-shadow" of the image sphere periphery as shown in Fig. 5. The width of this half-shadow can, however, be evaluated from the inflection point of the intensity signal and does therefore not introduce a significant error into the diameter determination. For the energy selection of the X-rays there are two opposite requirements. Higher X-ray energy will minimize the X-ray absorption in the high-pressure background gas of the autoclave. Lower X-ray energy will reduce the error in diameter determination by avoiding the X-rays passing through the sphere periphery, thus producing a diffuse, poorly defined image sphere as demonstrated by the intensity profile of transmitted X-rays in Fig. 6 [23] for a 500-μm UO_2 sphere. The X-ray absorption problem by high-pressure inert gas has been reduced by shortening the channels in the autoclave, i.e., by mounting the beryllium windows close to the heated sphere (Fig. 4). A further reduction is possible by changing from Ar to He.

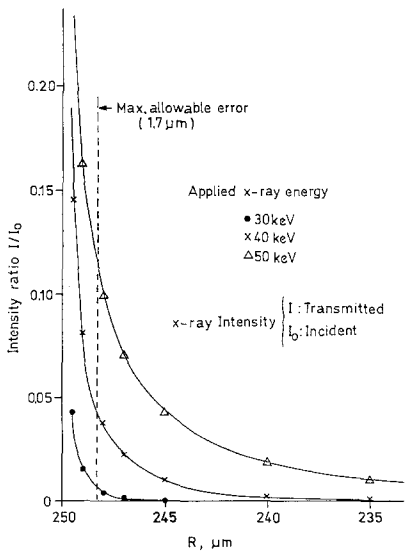

Fig. 6. Intensity profile of transmitted X-ray through a 500-μm UO_2 sphere.

6. HEAT CAPACITY MEASUREMENT

The rate at which a hot microsphere cools is given by the energy balance equation

$$\frac{4}{3} r^3 \pi \rho c_p \frac{dT}{dt} = -4\pi r^2 (\varepsilon \sigma T^4 + \alpha T) \tag{11}$$

where r, ρ, c_p, and ε are the radius, density, heat capacity, and total emittance of the sphere. The terms on the right-hand side are the loss rate due to radiation and convection. Convection losses at 5000 K are 0.2% of the radiation loss and can thus be neglected.[4] The energy balance equation reduces to

$$\frac{dT}{dt} = -\frac{3\varepsilon\sigma T^4}{\rho r c_p} \tag{12}$$

The solution by integration is

$$\left(\frac{T_i}{T}\right)^3 = 1 + \frac{9\varepsilon\sigma T_i^3}{\rho r c_p} t \tag{13}$$

where T_i is the initial temperature of the sphere. A plot of $1/T^3$ as a function of t allows to calculate c_p directly from the slope of the straight line, provided the total emittance, radius, and density are known. For typical values of UO_2 microspheres ($r = 0.5$ mm, $\rho \simeq 10\ \mathrm{g \cdot cm^{-3}}$, $c_p \simeq 160\ \mathrm{J \cdot mol^{-1} \cdot K^{-1}}$) [41, 42], the cooling time from an initial temperature of 5000 to 4000 K is of the order of 50 ms [1, 23].

Two effects due to finite conductivity and phase changes such as resolidification during the cooling cycle need special attention [23]. In Eq. (11) it is assumed that the sphere is at uniform temperature throughout the cooling phase, corresponding to infinite conductivity. The effect of finite thermal conductivity has been analyzed by a one-dimensional heat diffusion program to solve the heat diffusion equation [23]. It follows that for an accurate determination of the heat capacity of a UO_2 sphere up to 5000 K, due to its low thermal conductivity a sphere diameter of about 500 μm should not be exceeded.

A one-dimensional energy conservation equation was used to investigate the effect of density and phase changes on the heat capacity evaluation [23]. As soon as the sphere surface starts to resolidify the heat

[4] Figure 1.15, p. 43, TUAR-87 [43]; for corrections in case of forced convection in the ultrasonic field see pp. 39–48 [43].

capacity diverges to infinity and returns to the correct value when the solidification front reaches the center of the sphere. For an accurate evaluation of the heat capacity in the liquid phase measurements must be stopped, as expected, just before solidification starts. For measurements up to the melting point the sphere must be heated to a temperature just below the melting point and then allow to cool. This effect can, however, be useful to detect phase transitions such as the Bredig transition predicted for UO_2 [42].

7. CONCLUSION

The laser-autoclave technique (LAT) as a combination of pulsed multibeam laser heating under pressure, microsecond six-wavelength pyrometry, high-resolution X-ray shadow technique, and containment-free acoustic levitation proved to be well suited for the extension of spectral and total emissivity, density, and heat capacity measurements far beyond the melting and boiling point temperatures of refractory materials. Laser heating under pressure (LHP) has shown to eliminate the various phenomena of extreme rates of evaporation, charged particle emission, and liquid displacement under hydrodynamic flow conditions, observed in laser heating under vacuum (LHV) necessary for the study of the vaporization behavior of multicomponent systems [32].

Instabilities in the standing resonance wave pattern of acoustic levitation, caused by density changes of the inert gas during laser heating, can be compensated by increased radial retaining forces. The additional heat loss by forced convection in the ultrasonic field may be reduced by low conductive gases such as argon. The image resolution of the X-ray shadow technique necessary to fulfill the accuracy requirements of the measurement of the thermal expansion coefficient depends on the magnification factor and resolution of the converter foil. An improvement of the foil resolution (lines/mm) permits a reduction of the focal distance of the image plane and keeps the loss of X-ray intensity reasonably small.

The advantage of the laser-autoclave technique is its almost-unlimited applicability in high-temperature materials research due to containment-free heating by acoustic levitation regardless of the conductive or magnetic properties of the material.

Rapid melt quenching by a combination of this laser-autoclave technique with splat cooling techniques will widen our knowledge on metastable structure synthesis and amorphous metals research [1]. Even higher quench rates can be obtained by pulsed laser quenching when thin molten overlays are formed *in situ* on the spherical surfaces by short high-energy laser pulses in the nanosecond to picosecond range [1]. Rapid quenching

provides the means for tailoring properties, previously unobtainable, to meet specific material requirements [44].

Modifications of this technique and extension to critical point temperatures will, in addition, permit the study of critical phenomena and the measurement of critical-point temperatures [7, 10] hitherto not accessible by other techniques.

ACKNOWLEDGMENTS

The author would like to express his sincere thanks to his co-workers J.-F. Babelot, Dr. J.-P. Hiernaut, Dr. J. Magill, and P. Werner, to R. Beukers, F. Capone, W. Heinz, G. Kramer, M. Martellenghi, and R. Selfslag for their assistance in performing the experiments, to the visiting scientists Professor M. Hoch, University of Cincinnati, Dr. T. Matsui, University of Nagoya, Japan, and Dr. F. Sakuma, National Research Laboratory of Metrology, Japan, and for collaboration to Professor C. Cercignani and Dr. A. Frezzotti, Politecnico di Milano, Italy, Professor G. J. Hyland, University of Warwick, UK, and Professor G. Ruffino, University of Rome.

REFERENCES

1. R. W. Ohse, *Pure Appl. Chem.* **60**:309 (1988).
2. L. Brewer, in *IUPAC Handbook of Thermodynamic and Transport Properties of Alkali Metals*, R. W. Ohse, ed. (Blackwell Scientific, Oxford, 1985), p. xix.
3. L. Leibowitz and J. K. Fink, in *IUPAC Handbook of Thermodynamic and Transport Properties of Alkali Metals*, R. W. Ohse, ed. (Blackwell Scientific, Oxford, 1985), p. xxv.
4. R. W. Ohse, J.-F. Babelot, C. Cercignani, P. R. Kinsman, K. A. Long, J. Magill, and A. Scotti, *NBS Special Publication 561*, J. W. Hastie, ed. (NBS, Washington, D.C., 1979), Vol. 1, pp. 83–109; *J. Nucl. Mat.* **80**:232 (1979).
5. R. W. Ohse, J.-F. Babelot, A. Frezzotti, K. A. Long, J. Magill, C. Cercignani, and A. Scotti, *High Temp. Sci.* **13**:35 (1980).
6. H. K. Bowen, *Mater. Sci. Eng.* **44**:1 (1980).
7. J. Magill and R. W. Ohse, in *IUPAC Handbook of Thermodynamic and Transport Properties of Alkali Metals*, R. W. Ohse, ed. (Blackwell Scientific, Oxford, 1985), Chap. 2.5.1, pp. 73–103.
8. W. Haubold and S. Dreyer, in *IUPAC Handbook of Thermodynamic and Transport Properties of Alkali Metals*, R. W. Ohse, ed. (Blackwell Scientific, Oxford, 1985), Chap. 3.2, pp. 139–153.
9. M. Ross, D. A. Young, L. A. Glenn, and F. J. Rogers, in *IUPAC Handbook of Thermodynamic and Transport Properties of Alkali Metals*, R. W. Ohse, ed. (Blackwell Scientific, Oxford, 1985), Chap. 3.3, pp. 155–163.
10. R. W. Ohse, *J. Chem. Soc. Faraday Trans.* **2**(83):1235 (1987).

11. D. B. Dawson, in *IUPAC Handbook of Thermodynamic and Transport Properties of Alkali Metals*, R. W. Ohse, ed. (Blackwell Scientific, Oxford, 1985), Chap. 3.4, pp. 165–180.
12. W. Fischer, in *IUPAC Handbook of Thermodynamic and Transport Properties of Alkali Metals*, R. W. Ohse, ed. (Blackwell Scientific, Oxford, 1985), Chap. 3.5, pp. 181–201.
13. E. S. Pierson, K. A. Bonyhady, P. F. Dunn, R. D. Nathenson, and U. L. Uherka, in *IUPAC Handbook of Thermodynamic and Transport Properties of Alkali Metals*, R. W. Ohse, ed. (Blackwell Scientific, Oxford, 1985), Chap. 3.6, pp. 203–220.
14. A. P. Fraas and J. H. DeVan, in *IUPAC Handbook of Thermodynamic and Transport Properties of Alkali Metals*, R. W. Ohse, ed. (Blackwell Scientific, Oxford, 1985), Chap. 3.1, pp. 129–137.
15. C. C. Hsu, in *IUPAC Handbook of Thermodynamic and Transport Properties of Alkali Metals*, R. W. Ohse, ed. (Blackwell Scientific, Oxford, 1985), Chap. 2.5.2, pp. 105–110.
16. E. A. Fischer, P. R. Kinsman, and R. W. Ohse, *J. Nucl. Mat.* **59**:125 (1976).
17. L. Mistura, J. Magill, and R. W. Ohse, *J. Nucl. Mat.* **132**:95 (1985).
18. M. Ross, in *IUPAC Handbook of Thermodynamic and Transport Properties of Alkali Metals*, R. W. Ohse, ed. (Blackwell Scientific, Oxford, 1985), Chap. 2.6.1, pp. 111–115.
19. J. Th. M. DeHosson, in *IUPAC Handbook of Thermodynamic and Transport Properties of Alkali Metals*, R. W. Ohse, ed. (Blackwell Scientific, Oxford, 1985), Chap. 2.6.2, pp. 117–126.
20. K. Binder, in *Topics in Current Physics, 7* (Springer Verlag, Berlin, 1979).
21. I. R. McDonald, *J. Phys.* **C7**:1225 (1974).
22. R. W. Ohse, J.-F. Babelot, C. Cercignani, J.-P. Hiernaut, M. Hoch, G. J. Hyland, and J. Magill, *J. Nucl. Mat.* **130**:165 (1985).
23. R. W. Ohse, C. Cercignani, A. Frezzotti, J.-P. Hiernaut, M. Hoch, G. J. Hyland, J. Magill, T. Matsui, and P. Werner, *J. Metals* **37**:TMS Annual Meeting 29 (1985).
24. J. Magill, F. Capone, R. Beukers, P. Werner, and R. W. Ohse, *High Temp. High Press.* **19**:461 (1987).
25. R. W. Ohse, J.-F. Babelot, P. R. Kinsman, K. A. Long, and J. Magill, *High Temp. High Press.* **11**:225 (1979).
26. J-F. Babelot, J. Magill, and R. W. Ohse, in *Temperature, Its Measurement and Control in Science and Industry, Vol. V*, J. F. Schooley, ed. (Am. Inst. Phys., New York, 1982), pp. 439–446.
27. A. Cezairliyan, J.-F. Babelot, J. Magill, and R. W. Ohse, in *Theory and Practice of Radiation Thermometry*, D. P. DeWitt and G. D. Nutter, eds. (John Wiley, New York, 1988), Chap. 8, pp. 529–552.
28. J.-P. Hiernaut, R. Beukers, W. Heinz, R. Selfslag, M. Hoch, and R. W. Ohse, *High Temp. High Press.* **18**:617 (1986).
29. J.-P. Hiernaut, R. Beukers, M. Hoch, T. Matsui, and R. W. Ohse, *High Temp. High Press.* **18**:627 (1986).
30. G. R. Gathers, *UCRL*-92054 (Jan. 1985).
31. M. Ross, *Rep. Prog. Phys.* **48**:1 (1985).
32. R. W. Ohse, *Int. J. Thermophys.* **11**:771 (1990).
33. D. C. Menzies, TRG Report 1119(D) (UKAEA, London, 1966).
34. E. J. Robbins, TRG Report 1344(R) (UKAEA, London, 1966).
35. D. L. Booth, TRG Report 1759(R/X) (UKAEA, London, 1968/1974).
36. M. J. Gillan, in *Thermodynamics of Nuclear Materials* (IAEA, Vienna, 1975), Vol. I, pp. 269–285.
37. P. Browning, M. J. Gillan, and P. E. Potter, Report AERE-R 8129 (UKAEA, London, 1977).
38. T. F. Bott and J. F. Jackson, *Trans. Am. Nucl. Soc.* **26**:367 (1977).

39. R. W. Ostenson, *Nucl. Technol.* **43**:301 (1979).
40. E. A. Fischer, BNES Conference on Science and Technology of Fast Reactor Safety, Guernsey (May 1986).
41. K. A. Long, J.-F. Babelot, M. Hoch, J. Magill, and R. W. Ohse, *High Temp. High Press.* **12**:515 (1980).
42. G. J. Hyland and R. W. Ohse, *J. Nucl. Mat.* **140**:149 (1986).
43. Annual Report TUAR-87, Commission of the European Communities, Joint Research Center, European Institute for Transuranium Elements, EUR 11783 EN (1988).
44. R. W. Ohse, *The Industrial Laser Annual Handbook*, D. Belforte, L. Belleville and M. Levitt, eds. (PennWell Books, Laser Focus, Tulsa, Oklahoma, 1990).